View metadata, citation and similar papers at core.ac.uk
brought to you by CORE
provided by Elsevier - Publisher Connector

Cell, Vol. 93, 1105–1115, June 26, 1998, Copyright ©1998 by Cell Press

A 9 Å Resolution X-Ray Crystallographic Map of the Large Ribosomal Subunit

Nenad Ban,[1] Betty Freeborn,[2] Poul Nissen,[1] Pawel Penczek,[4,5] Robert A. Grassucci,[4] Robert Sweet,[6] Joachim Frank,[4,5] Peter B. Moore,[1,2] and Thomas A. Steitz[1,2,3,7]
[1]Department of Molecular Biophysics and Biochemistry
[2]Department of Chemistry
[3]Howard Hughes Medical Institute
Yale University
New Haven, Connecticut 06520-8114
[4]Wadsworth Center
New York State Department of Health
Albany, New York 12201-0509
[5]Department of Biomedical Sciences
State University of New York
Albany, New York 12201-0509
[6]Department of Biology
Brookhaven National Laboratory
Upton, New York 11973

Summary

The 50S subunit of the ribosome catalyzes the peptidyl-transferase reaction of protein synthesis. We have generated X-ray crystallographic electron density maps of the large ribosomal subunit from *Haloarcula marismortui* at various resolutions up to 9 Å using data from crystals that diffract to 3 Å. Positioning a 20 Å resolution EM image of these particles in the crystal lattice produced phases accurate enough to locate the bound heavy atoms in three derivatives using difference Fourier maps, thus demonstrating the correctness of the EM model and its placement in the unit cell. At 20 Å resolution, the X-ray map is similar to the EM map; however, at 9 Å it reveals long, continuous, but branched features whose shape, diameter, and right-handed twist are consistent with segments of double-helical RNA that crisscross the subunit.

Introduction

In all organisms, messenger-directed protein synthesis is catalyzed by ribonucleoprotein particles called ribosomes. Bacterial ribosomes sediment at about 70S and consist of two nonequivalent subunits: a small, 30S subunit and a large, 50S subunit. The latter has a molecular mass of about 1.5×10^6 Da and catalyzes peptide bond formation, possibly functioning as a ribozyme (Noller et al., 1992). The 50S subunit contains a 2900 nt RNA and a 120 nt RNA and about 33 different proteins (Wittmann-Liebold, 1986). If the structure of this macromolecular assembly and its substrate complexes were solved at atomic resolution, a significant increase in the understanding of the mechanism of protein synthesis would result, as well as valuable insights into RNA structure and RNA–protein interactions.

All of the current information on the ribosome structure derives from physical and chemical methods capable of producing relatively low-resolution information. In the 1970s, the shape and quaternary organization of ribosomes were illuminated by electron microscopy (EM) (Oakes et al., 1986; Stoeffler and Stoeffler-Meilicke, 1986), and by the end of the 1980s, the positions of all of the proteins in the 30S subunit and many of the proteins in the 50S subunit had been determined by neutron scattering (Capel et al., 1987; May et al., 1992). Recent advances in single-particle cryo-EM have led to three-dimensional reconstructions of the *Escherichia coli* 70S ribosome and its complexes with tRNAs and elongation factors at resolutions between 15 and 25 Å (Frank et al., 1995a, 1995b; Stark et al., 1995, 1997a, 1997b; Agrawal et al., 1996; Zhu et al., 1997; Malhotra et al., 1998). Detailed models of the conformation of 16S RNA in the small subunit have been proposed based on this kind of structural information and RNA footprinting data (Malhotra and Harvey, 1994; Noller et al., 1995; Mueller and Brimacombe, 1997a, 1997b; Mueller et al., 1997). While these models integrate much of the structural and functional information available on the ribosome, studies of other, less complicated enzymes leave little doubt that only high-resolution crystal structures of the ribosome will yield accurate models that are sufficiently detailed so that the mechanisms of processes such as substrate recognition, peptide bond formation, and translocation can be fully understood.

Ada Yonath and coworkers made a seminal contribution to the quest for a high-resolution structure of the ribosome by obtaining the first crystals of ribosomes and of ribosomal subunits, and by discovering crystals of the *Haloarcula marismortui* large subunit that diffract beyond 3 Å resolution (Yonath et al., 1980; Shevack et al., 1985; van Bohlen et al., 1991; Franceschi et al., 1993). This accomplishment established that, in principle, an atomic level structure of the ribosome can be determined using X-ray crystallography. However, the published electron density maps of the *H. marismortui* 50S subunit, which were based on X-ray diffraction data from crystals derivatized by heavy atom cluster compounds, do not show the continuous density features expected (Schlunzen et al., 1995). For this reason, we decided to pursue a strategy that depends on using EM maps to phase the X-ray diffraction data at low resolution in order to assist in the location of heavy atoms, as Harrison and coworkers did in their crystallographic studies of tomato bushy stunt virus more than 20 years ago (Jack et al., 1975).

Although many high-resolution crystal structures of spherical viruses, which are larger than the ribosome, have been determined during the last two decades, the structure of the ribosome presents a more formidable problem because it combines large size with lack of symmetry. The high symmetry of viruses helped their structure determination in two ways: the asymmetric unit of a virus crystal is only a small fraction of the entire particle; furthermore, averaging of the identical subunits in the asymmetric unit results in stunning map improvement even if the initial heavy atom phased map is poor

[7]To whom correspondence should be addressed.

(Rossmann, 1995). However, averaging cannot be used when there is only a single 1.5 million molecular weight particle in the asymmetric unit. In order to obtain measurable diffraction differences from heavy atoms bound to such a large asymmetric structure, a very large number of single heavy atoms must be bound. As an approach to this problem, heavy atom cluster compounds, which scatter like super heavy atoms at very low resolution but become decreasingly effective at modestly higher resolutions, have been used to increase the size of intensity differences greatly (Ladenstein et al., 1987; O'Halloran et al., 1987; Thygesen et al., 1996; Knablein et al., 1997; Neuefeind et al., 1997). Whatever heavy atom compounds are used, the essential first step in solving the crystal structure of the ribosome is to locate correctly and model bound heavy atoms in several derivatized ribosome crystals, which we have now successfully achieved.

We present here X-ray crystallographically determined electron density maps of the *H. marismortui* large ribosomal subunit calculated at resolutions between 20 Å and 9 Å; they begin to unveil the molecular architecture that underlies this large, ribonucleoprotein complex. The X-ray maps were calculated using phases determined by multiple isomorphous replacement and anomalous scattering (MIRAS) from three heavy atom derivatives. Important to the success of this study was the molecular replacement of a 20 Å resolution EM map into the crystal cell, which provided initial phases for low-resolution reflections. Using these EM-derived phases, it was possible to locate the high-occupancy sites in heavy atom-derivatized crystals in difference Fourier maps and thus to initiate the process of heavy atom refinement. The X-ray map calculated at 20 Å resolution shares many features with the 20 Å resolution EM map, but the region believed to contain ribosomal protein L1 is oriented differently. Although protein cannot be clearly distinguished from RNA at 9 Å resolution, the map contains many continuously connected and branched densities, which are about 20 Å in diameter in many places, consistent with their representing an RNA double helix. Further, a right-handed twist arising from duplex backbone can be seen. Thus, we believe that a critical step has been taken on the path leading to an electron density map of the large ribosomal subunit that can be interpreted in atomic detail.

Results

Electron Microscopic Images

Two electron microscopic reconstructions of large ribosomal subunits were used in the course of this work. The 50S subunit reconstruction used initially was abstracted from a 23 Å resolution map of the intact 70S ribosome from *E. coli* (Frank et al., 1995a) using a lower resolution map of the *E. coli* 30S ribosomal subunit (Lata et al., 1996) as a guide to determine the location of the boundary between the 50S and 30S subunits. Subsequently, a reconstruction of isolated large ribosomal subunits from *H. marismortui* was done (see Experimental Procedures) because it was deemed more appropriate for these crystallographic studies. That reconstruction was derived from 13,170 images of individual particles taken at two levels of defocus under ionic conditions similar to those used for crystal growth. *H. marismortui* image orientations were determined initially by comparison with images computed from the *E. coli* 50S reconstruction just described, and then refined. Figure 1 shows the dependence of the Fourier shell correlation coefficient (FSC) of this reconstruction as a function of resolution (Böttcher et al., 1997). In an ideal reconstruction, the FSC would be 1.0 out to some limiting value and would then fall to 0. In this case, it begins to fall below 1.0 at about 50 Å resolution, reaches 0.5 at 20 Å resolution, and is nonzero to nearly 12 Å. Thus, while the nominal resolution of this map is 20 Å, it clearly contains useful information to higher resolution (see below).

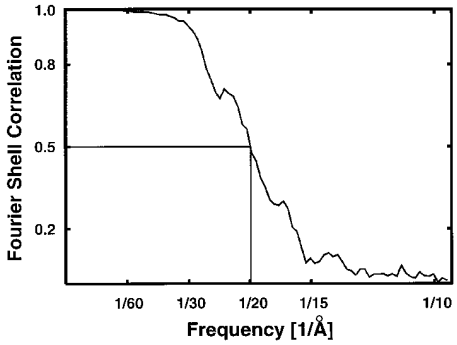

Figure 1. Resolution Estimation of EM Reconstruction of the HM 50S Subunit

Nominal resolution is 20 Å for a FSC cut-off level 0.5 (Böttcher et al., 1997). FSC: $\Sigma_R[F_1(R)\ F_2(R)]/(\Sigma_R|F_1(R)|^2\Sigma_R|F_2(R)|^2)^{1/2}$, where R is the shell radius in Fourier space; F1 and F2 are Fourier transforms of 3D structures calculated from two randomly divided subsets of the available EM projection data. The summation is carried over shells in Fourier space.

Molecular Replacement

Using modified forms of the molecular replacement procedures implemented by the computer programs X-PLOR and CNS, EM reconstructions of the large ribosomal subunit were positioned in the crystal unit cell with good packing. The crystals of *Haloarcula marismortui* large ribosomal subunits (HM 50S) used in this study were grown following procedures described by Yonath and coworkers (van Bohlen et al., 1991). They are orthorhombic, space group $C222_1$, and with unit cell dimensions of: a = 210, b = 300, c = 570 Å. Although these crystals diffract to better than 3.5 Å resolution, the data used for this study were measured to 7.0 Å resolution at Brookhaven National Laboratory (Table 1).

After rigid body refinement, the best molecular replacement solution found for EC 50S had an R factor of 0.45 and a correlation coefficient of 0.43 for reflections between 60 and 30 Å resolution. The resulting unit cell packing shows no unacceptable contacts or overlaps between subunits. Subsequently, when the HM 50S EM reconstruction became available, the rotation and translation searches were repeated and the same packing solution was obtained (Figure 2). Encouragingly, the signal-to-noise ratio was better in all steps (Table 2); the R factor was lower (0.39) and the correlation coefficient

Table 1. Summary of Molecular Replacement Statistics

Direct Rotation Search (25.0–80.0 Å)			
	Correct Solution (RF)	False Peak (RF)	S/N
H. marismortui	0.18	0.15	1.2
E. coli	0.20	0.22	0.92
PC Refinement of the Rotation Function Solutions (25.0–80.0 Å)			
H. marismortui	0.14	0.074	1.9
E. coli	0.14	0.087	1.6
Translation Search (25.0–80.0 Å)			
	Correct Solution (E2E2)	False Peak (E2E2)	S/N
H. marismortui	0.48	0.36	1.33
E. coli	0.44	0.35	1.26
Final Statistics (60.0–30.0 Å; 360 reflections)			
	R factor	Correlation Coefficient	
H. marismortui	0.39	0.51	
E. coli	0.45	0.43	

E2E2, Patterson correlation coefficient, where E is a normalized structure factor as defined in X-PLOR; S/N, signal to noise; RF, Rotation function value as defined in X-PLOR; R factor, $\Sigma_{hkl}(||Fobs_{hkl}| - |Fcalc_{hkl}||)/|Fobs_{hkl}|$, where $|Fobs_{hkl}|$ and $|Fcalc_{hkl}|$ are the observed and calculated structure factor amplitudes.

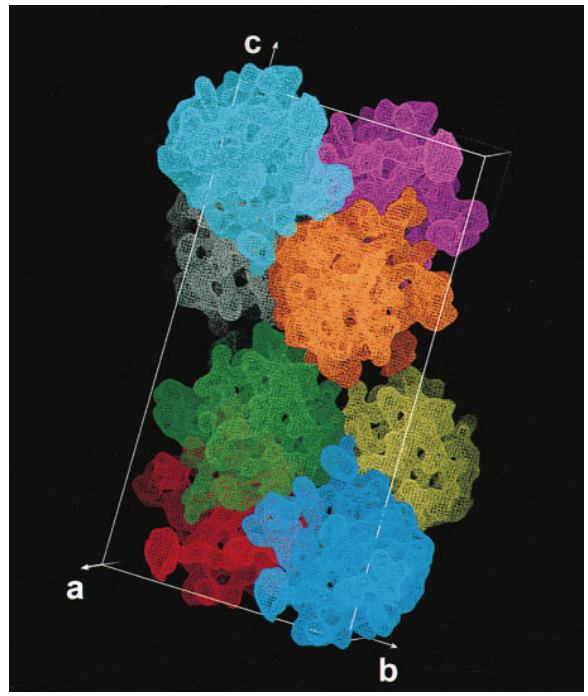

Figure 2. The Packing of *H. marismortui* 50S Subunits in the Orthorhombic Unit Cell Viewed Approximately down Its **a** Axis

The eight subunits related by crystallographic symmetry are shown in different colors. Less extensive crystallographic contacts are formed between subunits colored green and orange, while green/red and orange/lavender subunit pairs have extensive contact surfaces.

was higher (0.51). Both of these packing studies were done using step function representations of EM maps (see Experimental Procedures) similar to the procedures described by Podjarni and Urzhumtsev (1997). Even better phases resulted when continuous EM-determined electron density was positioned in the unit cell. The W18 difference Fourier peak increased from 13 σ to 14 σ (see below) while the R factor decreased from 44% to 41% for the 1322 reflections between 100 and 20 Å resolution.

HM 50S subunits pack in this C-centered, orthorhombic cell in tight pairs that are related by a crystallographic 2-fold axis parallel to the **b** direction. The L7/L12 regions of subunits related by that dyad axis interact with each other at the interface between the two subunits. There are only weak contacts between molecules related by the crystallographic 2-fold axis along the **a** axis of the unit cell.

Heavy Atom Derivatives

The positions of the major heavy atom binding sites in the three different derivatives were found using difference Patterson maps as well as difference electron density maps, calculated with EM-derived phases. The first derivative obtained was prepared by soaking crystals in solutions containing an 18-atom tungsten cluster compound (W18). The position of the highest occupancy W18 binding site was evident in the three Harker sections of a 14 Å resolution difference Patterson map, which contained correlated peaks at about twice the noise level. Recently, data were recollected from this derivative with the X-ray wavelength set to the tungsten absorption edge, and the combined isomorphous and anomalous difference Patterson map calculated contained 7 σ peaks in the same positions (Figure 3a).

We were able to verify simultaneously both the correctness of the molecular replacement solution shown in Figure 2 as well as our interpretations of derivative difference Patterson maps by calculating difference electron density maps, using EM-derived phases. For example, a difference Fourier map of the W18 derivative calculated using X-ray amplitudes between 35 and 14 Å resolution and phases derived from the EC 50S reconstruction contained a 6 σ peak at the expected position, whereas a similar map calculated using phases derived from the HM 50S reconstruction showed a 13 σ peak (Figure 3b). The dramatic improvement in the signal-to-noise ratio obtained using the HM 50S reconstruction shows that it is a significantly more accurate representation of the subunits in these crystals.

To examine the resolution limit of phasing provided by EM reconstructions, difference isomorphous Fourier maps were calculated at various resolution ranges and the heights of the heavy atom peaks compared. The peak in Figure 3b remained the strongest peak in a difference map calculated using data between 18 and 14 Å, suggesting that the EM map is still generating useful phase information at this resolution, which is significantly higher than its nominal 20 Å resolution, consistent with Figure 1.

A second heavy atom derivative containing a bound W11 compound produced difference Patterson maps in which one major site could be identified, and several additional sites were found in difference Fourier maps. The major sites of a third derivative, prepared using a

Table 2. Data Collection and Phasing Statistics

Data Collection

	Native	W18	W11	Ta
Soaking time		6 days	2 days	5 days
Cluster concentration (mM)		1.0	1.0	1.0
Wavelength (Å)	1.21	1.21	1.21	1.25
Resolution	100–7.2	100–7.0	100–7.0	100–7.0
Observations				
Total	98,000	204,087	191,540	15,1534
Unique	26,324	50,576	57,103	56,172
Completeness	98.3	92.7	99.2	94.2
R_{sym}	11.1	4.5	5.2	5.5
No. Sites		7	12	10
R_{iso}		23.9	27.3	19.5
$I/\sigma I$ (highest resolution bin)	11.1 (2.8)	31.7 (13.8)	24.4 (7.7)	21.6 (9.4)

MIRAS Phasing Statistics

	Resolution Shells (Å)—~6400 Reflections per Bin					
	90.0	14.2	11.3	9.9	9.0	Total (25,540 reflections)
W18						
Phasing power	1.28	1.13	0.77	0.56		1.10
R_{cullis} (centric)	0.67	0.78	0.87	0.91		0.72
W11						
Phasing power	1.4	1.2	0.85	0.63		1.15
R_{cullis} (centric)	0.65	0.78	0.83	0.88		0.70
Ta						
Phasing power	0.83	0.84	0.64	0.58		0.75
R_{cullis} (centric)	0.79	0.86	0.92	0.91		0.83
Mean figure of merit	0.82	0.71	0.54	0.43		0.63

R_{iso}: $\Sigma|F_{PH}-F_P|/\Sigma F_{PH}$, where F_{PH} and F_P are the derivative and the native structure factor amplitudes, respectively. R_{sym}: $\Sigma\Sigma_i|I_{(h)}-I_{(h)i}|/\Sigma\Sigma_i I_{(h)i}$, where $I_{(h)}$ is the mean intensity. Phasing power: rms isomorphous difference divided by the rms residual lack of closure. R_{cullis}: $\Sigma(||F_{PH}-F_P|-|F_{H(calc)}||)/\Sigma|F_{PH}-F_P|$, where F_{PH} is the structure factor of the derivative and F_P is that of the native data. The summation is valid only for centric reflections.

tantalum cluster compound, were identified by a combination of anomalous and isomorphous difference Fourier maps.

The positions and occupancies of bound clusters were refined as rigid bodies by maximum likelihood methods to minimize the lack of closure, and phases were calculated using multiple isomorphous replacement and anomalous scattering (MIRAS). Using these phases, more accurate difference Fourier maps were computed that revealed the locations of numerous minor cluster binding sites in all three derivatives. Using the positions of the major and minor heavy atom binding sites, difference Patterson maps were computed that match the major features in the corresponding experimental difference Patterson maps (Figure 3a). The phasing power of each of the three derivatives and the average figure of merit examined as a function of resolution suggest that the quality of the MIRAS phasing is excellent to 12.5 Å but drops significantly beyond 9 Å. For this reason, a 9 Å resolution electron density map was calculated using MIRAS phasing from all three derivatives.

The Structure of the 50S Subunit

The X-ray crystallographically derived electron density map of the *H. marismortui* large ribosomal subunit resembles the electron microscopic reconstruction of the same particle. Comparison of a surface rendering of the HM 50S EM 20 Å resolution reconstruction (Figure 4a) with a similar rendering of a 20 Å resolution map derived from X-ray data alone (Figure 4b) shows that both structures have the same overall shape and density features. The resolution of the X-ray map appears substantially higher, however, presumably because the amplitudes of its high-resolution components are larger. Nevertheless, most of the structural characteristics of the large ribosomal subunit previously visualized by EM reconstruction (Frank et al., 1995a) and identified biochemically by immunoelectron microscopy (Oakes et al., 1986) are easily recognized (Figures 4b and 4c). The most obvious differences involve the region of the 50S subunit known to include ribosomal protein L1 and a region where the 50S subunit contacts the small subunit. The X-ray map suggests that the positions of these protrusions are shifted in the crystal, which may mean that these domains are capable of adopting several different conformations.

Comparison of sections through the crystallographic unit cell taken from maps computed using X-ray intensities and either EM-derived phases (Figure 5b) or X-ray-derived phases (Figure 5a) show some similar features of continuous electron density. Since these two maps have only the X-ray amplitudes in common, we conclude that both the EM and the X-ray-derived phases are basically correct.

X-ray electron density maps calculated at 14 Å (Figures 6a and 6b) and 9 Å resolution (Figures 4c, 4d, and 6c) show long, continuous rods of electron density that

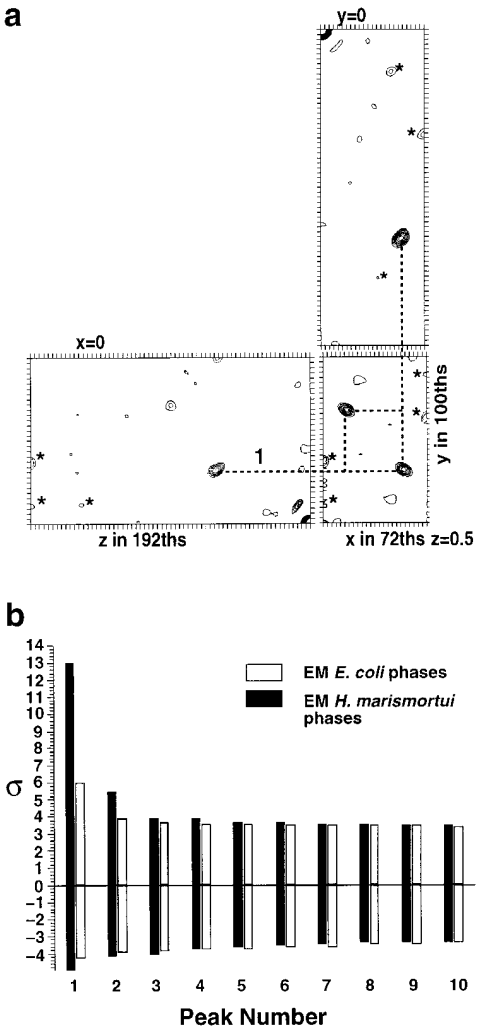

Figure 3. Heavy Atom Locations Determined by Difference Patterson and Difference Fourier Maps

(a) The three Harker sections from a combined isomorphous-anomalous difference Patterson map of the W18 derivatized crystals of the *Haloarcula marismortui* 50S ribosomal subunit with the predicted positions indicated. The map is contoured at 2 σ with 1 σ increments. The number 1 and the stars indicate the Patterson peaks expected from the major and minor sites, respectively.

(b) Histograms of the largest positive and negative isomorphous peaks identified in the 14 Å isomorphous difference Fourier maps of the HM 50S subunit crystals using phases derived from the HM 50S reconstruction or the EC 50S reconstruction (Frank et al., 1995a). The phases were weighted according to the SigmaA scheme for the data between 35 and 14 Å resolution.

are bent, branched in places, about 20 Å in diameter, and have distinct, right-handed spiral features expected from double-stranded RNA (Figure 6c). These density features are likely to represent the branched, double-helical RNA that constitutes about two-thirds of the subunit's mass. There are regions where the presumed RNA density is well separated from other features and regions of more extensive, unresolved density that could correspond to more tightly packed RNA helices and/or clusters of protein subunits with RNA (Figures 6a and 6b). Aside from suggesting where protein L1 might be, we have made no attempt to assign density to protein separately from RNA, since the resolution is insufficient. Among the features visible on the side facing the 30S subunit, several protrusions are seen whose locations suggest that they furnish some of the intersubunit bridges observed in the cryo-EM map of the *E. coli* 70S ribosome (Frank et al., 1995a, 1995b).

Discussion

We conclude that cryo-EM reconstructions of single particles can be used to phase the X-ray diffraction amplitudes of crystals of macromolecular assemblies in order to locate bound heavy atoms in derivative crystals. It is clear that the EM maps obtained from *H. marismortui* are excellent representations of the 50S subunit in the crystals studied here. Further, since the 20 Å resolution maps generated using either EM or X-ray-derived phases are similar, both methods must be producing correct structures at this resolution. In contrast, our all-X-ray map does not resemble the previously published X-ray electron density map of the *H. marismortui* large ribosomal subunit, which had a nominal resolution at 7 Å, nor is the packing of subunits in the unit cell described here the same as that deduced in that study from a solvent flattened map (Schlunzen et al., 1995).

The EM reconstruction of the large subunit from *H. marismortui* is a significantly better model for the subunit in these crystals than the EM map of the 50S subunit carved out of the reconstruction of the 70S ribosome from *E. coli*, as judged by molecular replacement statistics and by the increase in size of the difference Fourier peak for the W18 cluster. There are several possible explanations for the differences between these two EM maps. Perhaps the most likely is that the structures of the eubacterial and archaebacterial ribosomes are significantly different at low resolution, as the sequence differences between their RNAs and proteins might imply (Wittmann-Liebold et al., 1990; Woese, 1996). It is also possible that there are conformational differences between isolated 50S subunits and 50S subunits complexed with small subunits. Alternatively, it could be that we failed to distinguish density arising from the 50S subunit from density belonging to 30S subunits correctly when abstracting the 50S map from maps of the whole *E. coli* ribosome.

In order to help identify electron density features in the 9 Å resolution HM 50S map, it has been compared with a 9 Å resolution map of 5S RNA fragment 1 calculated from its atomic coordinates (Correll et al., 1997). Many of the strands in the *H. marismortui* 50S map have distinct, right-handed spiral ridges that resemble the ridges in the 5S fragment map that arise from the duplex backbone. Presumably, the spiral ridges in the HM 50S map also represent the sugar phosphate backbone. In both maps, the spacings between the backbone ridges vary from that of A-form RNA due to the presence of non-Watson-Crick base pairs. The right-handedness of the strands in the HM 50S map proves that the hand of the ribosome was indeed correctly determined by earlier EM studies (Leonard and Lake, 1979) and by the method of single-particle reconstruction (Radermacher et al., 1987).

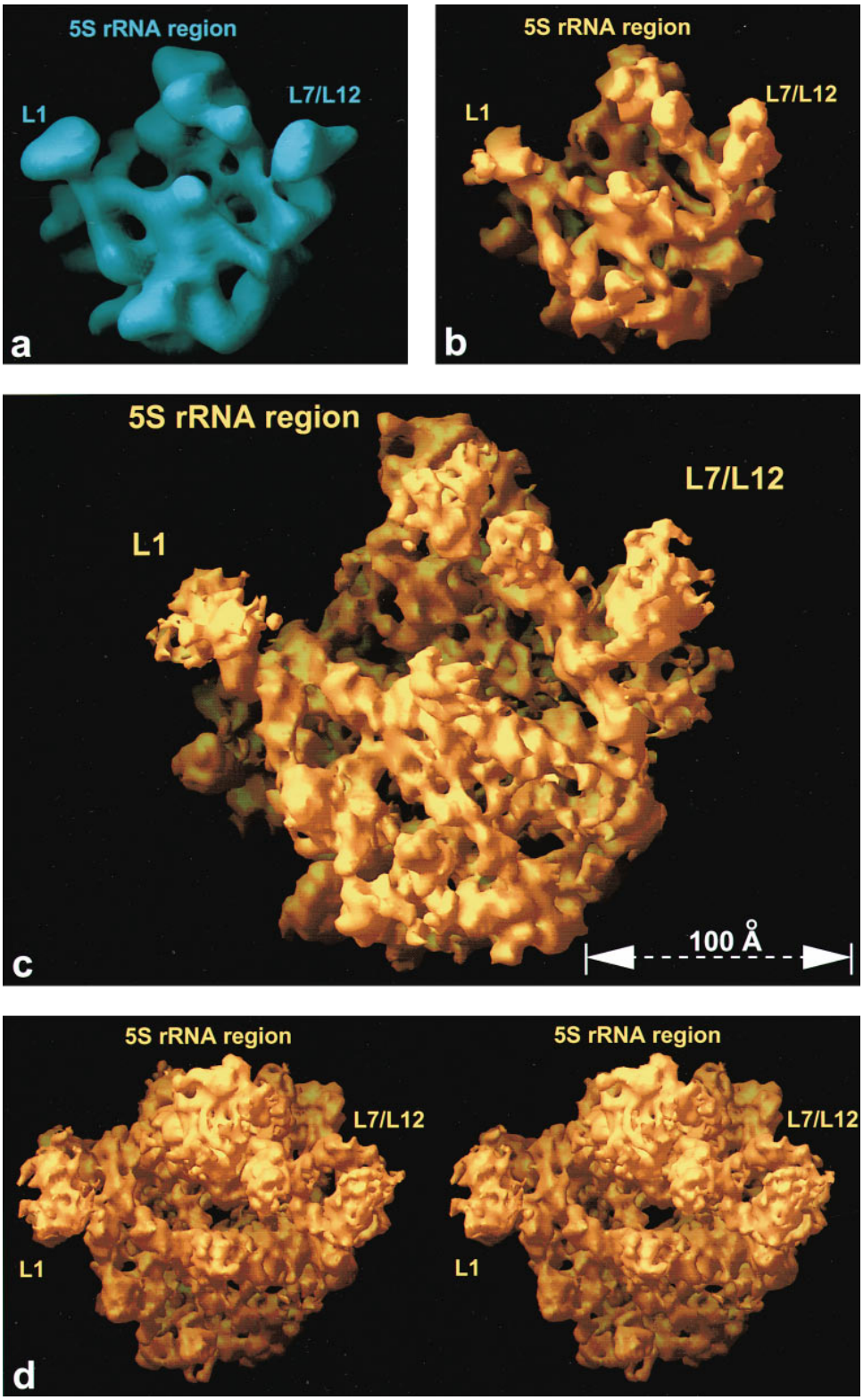

Figure 4. Comparison of the 20 Å Resolution EM Reconstruction with Both 20 Å and 12 Å Resolution X-Ray Maps of the HM 50S Subunit

(a) A surface rendering of the EM reconstruction of the 50S subunit at about 20 Å resolution. This structure was used in the molecular replacement study. Previously identified features such as the position of ribosomal protein L1, the L7/L12 region, and the 5S ribosomal RNA in the central protuberance are labeled. The large subunit is shown in the crown view from the side that interacts with the 30S subunit.

(b) A surface rendition of a 20 Å resolution "all X-ray" electron density map calculated using phases derived by MIRAS using three heavyatom derivatives. The volume occupied by the map contoured at this level is about 85% of the expected volume of the large ribosomal subunit calculated from molecular mass. The subunit is shown in the same view as in (a).

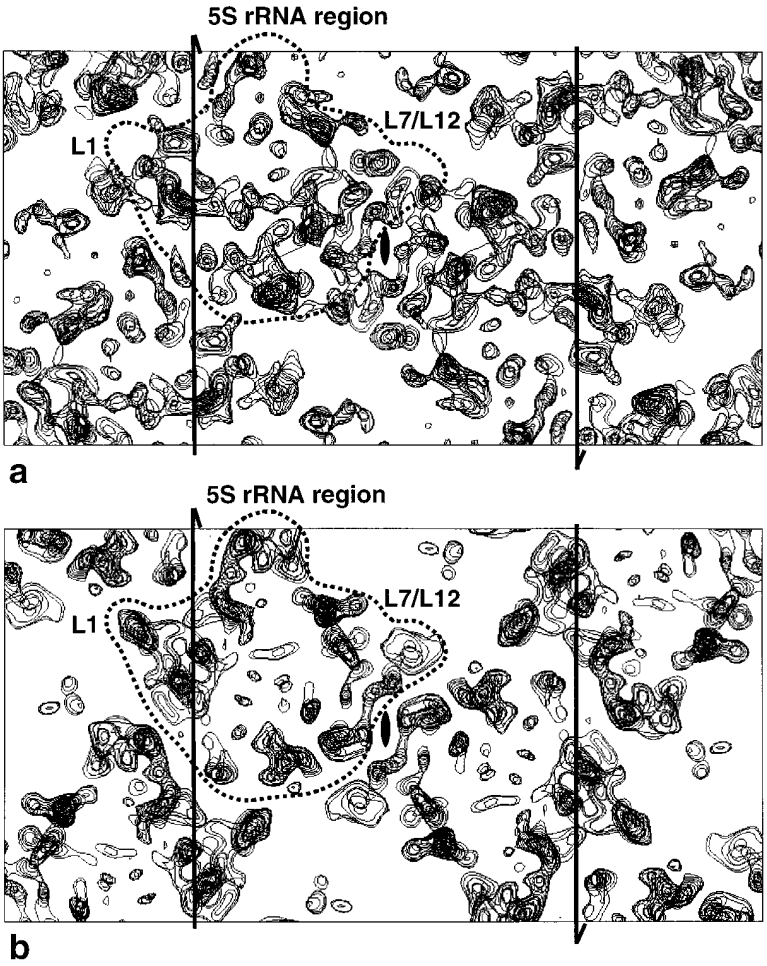

Figure 5. Comparison of HM 50S Electron Density Maps Calculated Using X-Ray- or EM-Derived Phases and X-Ray Amplitudes

(a) An approximately 20 Å thick superposition of sections through the HM 50S electron density map, calculated at 20 Å resolution using MIRAS X-ray phasing derived from three derivatives (Table 2) with no solvent flattening. The dotted line represents the 50S subunit envelope derived from the EM map positions by molecular replacement. The map shows a clear solvent and subunit boundary, and many of the features, such as the continuous density near the central 2-fold axis, are visible in both the X-ray and EM-phased maps. The slice through the unit cell was chosen to portray prominent features, such as the L1 region, central protuberance, and the L7/L12 region.

(b) For comparison, the superposition of the same sections of a map calculated using HM 50S EM-derived phases and observed X-ray diffraction amplitudes is shown.

Since rods of electron density, presumed to be RNA, crisscross the entire large subunit, it is obvious that the general architectural principle of this protein–nucleic acid assembly is distinctly different from those of nucleosomes or viruses. RNA and protein are intermingled, rather than the nucleic acid being wrapped around a protein core or encased in a protein shell. Present models of the small ribosomal subunit based on neutron scattering, chemical modification, and cryo-EM likewise place the proteins within a forest of RNA helices (Malhotra and Harvey, 1994; Noller et al., 1995; Mueller and Brimacombe, 1997a, 1997b; Mueller et al., 1997). It appears (Figures 6a and 6b) that the 50S ribosome structure is formed by struts of RNA rods whose branching cross-links the struts. Proteins may serve to stabilize further the branched RNA scaffold.

Rotation of the map shown in Figure 4c by about 50 degrees around its horizontal axis reveals a tunnel (Figure 4d). This tunnel aligns with tunnels observed in cryo-EM maps of large ribosomal subunits from *H. marismortui* (this study), *E. coli* (Frank et al., 1995a; Malhotra et al., 1998), and yeast (Beckmann et al., 1997; Verschoor et al., 1998), when the subunits themselves are aligned. A similar observation was made by Dube et al. (1998), who compared ribosomes from rat liver and *E. coli*. The tunnel, presumably identical with that found by Yonath et al. (1987) in the 70S ribosome and by Milligan and Unwin (1986) in the 80S, is thought to conduct the nascent polypeptide chain from the peptidyltransferase center to a point where it exits the ribosome (reviewed by Eisenstein et al., 1994). In agreement with this hypothesis, the acceptor end of the P-site-bound-fMet-tRNA is found in the immediate vicinity (~15 Å) of the tunnel entrance (Malhotra et al., 1998), and the tunnel exit, on the back of the large subunit, was found to align with the central pore of the Sec61 channel in yeast (Beckmann et al., 1997). According to this interpretation, the peptidyltransferase center must be in the immediate neighborhood of the tunnel entrance shown in the X-ray-derived map in Figure 4d.

(c) An X-ray-phased 9 Å resolution map oriented as in (a).

(d) The same map as in (c) rotated by about 50° about a horizontal axis to show a tunnel that lies at the back of the peptidyltransferase cleft in the approximate center of the particle. All maps are displayed by RIBBONS, a crystallographic molecular graphics program (Carson, 1991).

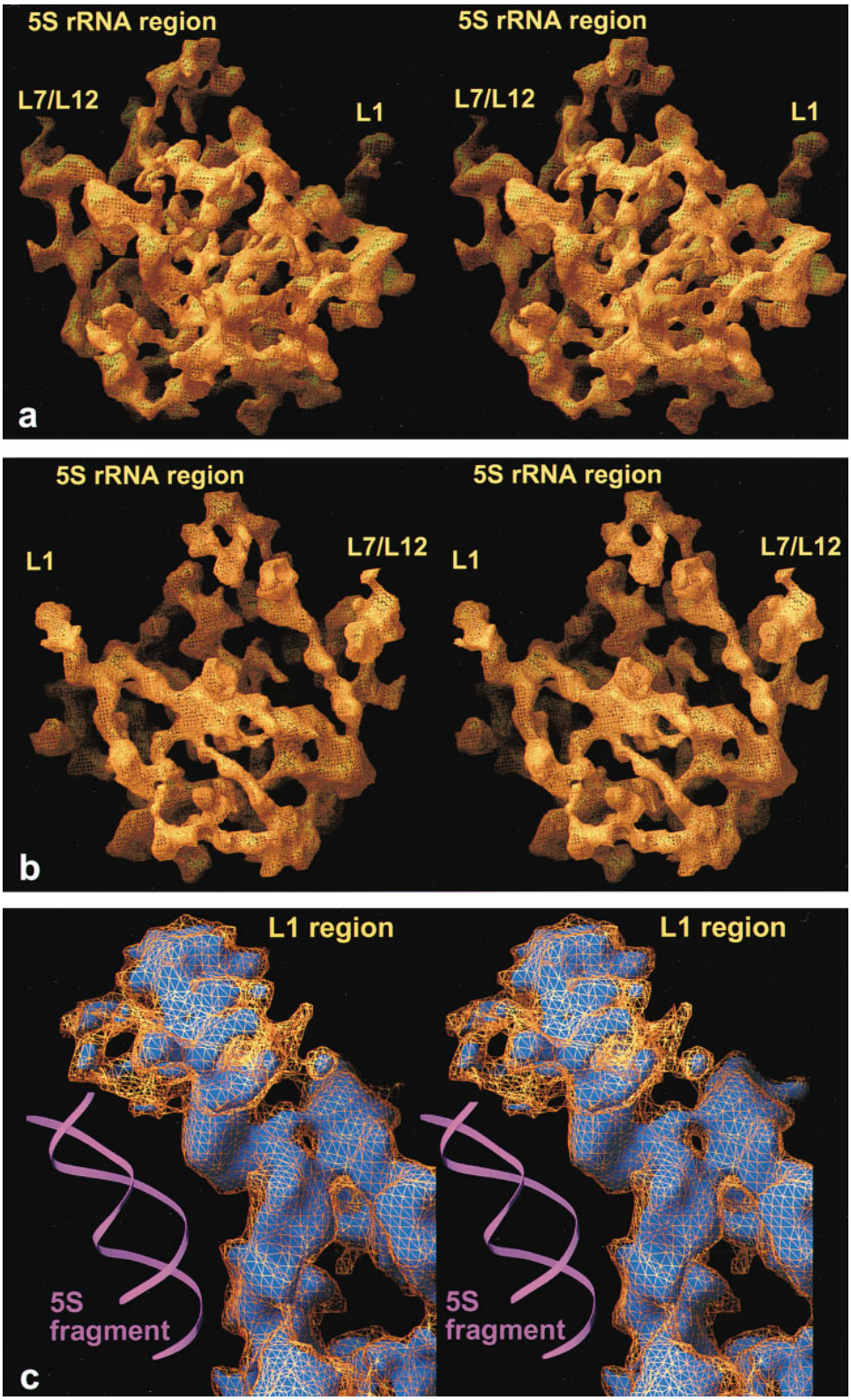

Figure 6. X-Ray Maps at 14 and 9 Å Resolution

(a) The MIRAS map in the crown view at 14 Å resolution shown in stereo from the side opposite the 30S subunit. Previously identified features such as ribosomal protein L1, L7/L12 region, and 5S ribosomal RNA in the central protuberance are labeled. To show the underlying strut-like architecture, the map is contoured at a high-density level and all density not connected has been removed.

(b) The same MIRAS map shown in the crown view.

This X-ray crystallographic map of a ribosomal subunit shows electron density features expected from other structural studies. Although the quality of its phasing and the resulting electron density diminishes at resolutions higher than 9–10 Å, it constitutes an important beachhead for launching an attack on the structure of the ribosome at higher resolution. These 9 Å resolution phases should make it possible to find the heavy atom sites in derivatives containing large numbers of single heavy atoms by difference electron density maps. Additionally, improved modeling of the heavy atom cluster compounds may improve the phasing quality at higher resolution. Thus, we anticipate obtaining higher resolution insights into the ribosome's structure and function in the near future.

Abbreviations

Abbreviations are as follows: HM50S, *Haloarcula marismortui* large ribosomal subunit; EC50S, *Escherichia coli* large ribosomal subunit; EM, electron microscopy SIR(AS) single isomorphous replacement (anomalous scattering); MIR(AS), multiple isomorphous replacement (anomalous scattering); W18, heavy atom cluster $(AsW_9O_{33})_2(PhSn)_4$; W11, heavy atom cluster $Cs_5(PW_{11}O_{39}\{Rh_2(CH_3COO)_2\})$; Ta, heavy atom cluster $Ta_6Br_{12}{}^{+2}$; and L7/L12, the region of the ribosome where proteins L7 and L12 are located.

Experimental Procedures

Cells and Ribosomes

H. marismortui (ATCC 43049) was grown on a slightly modified version of ATCC culture medium 1230, which was supplemented with 4.3 g of yeast extract, 5.1 g of Tris, and 3.4 g of glucose per liter. Bacteria were grown at 37°C to an OD_{550nm} between 1.0 and 2.2. They were harvested by centrifugation and stored at −80°C. Cells were ruptured using a French press. Ribosomes were prepared from lysates by centrifugation, and subunits were isolated on sucrose gradients (Shevack et al., 1985).

Electron Microscopy

Grids were prepared for cryomicroscopy using standard methods (Dubochet et al., 1988; Wagenknecht et al., 1988). The sample was diluted to an optical density at 260 nm of 1.2 immediately before preparation of cryo grids to prevent aggregation, and it was applied onto grids and flash-frozen for cryo-electron microscopy. Micrographs were recorded using low-dose protocols on a Philips EM420 microscope at a magnification of 52,200× ± 2%, which was established using a tobacco mosaic virus as a standard.

Image Processing

Micrographs were checked for drift, astigmatism, and presence of Thon rings by optical diffraction. Scanning was done with a step size of 25 μm, which corresponds to 4.79 Å on the ribosome, using a Perkin Elmer PDS 1010A microdensitometer. A total of 40 micrographs were used, grouped into two defocus settings: 1.25 and 1.80 μm. HM 50S subunit images were automatically selected from micrographs by comparing them with a reference set of 87 quasi-evenly spaced projection images (Penczek et al., 1994) of the 50S subunit portion of a 70S *E. coli* ribosome reconstruction (Frank et al., 1995a). This 50S image was carved out of the 70S map using a lower resolution reconstruction of the 30S subunit from *E. coli* (Lata et al., 1996). The number of particles selected was 6150 for 1.25 μm group and 7020 for 2.80 μm group. For each defocus group, one cycle of a 3D projection alignment procedure (Penczek et al., 1994) was applied, and a merged, contrast transfer function (CTF)–corrected reconstruction was computed as described earlier (Zhu et al., 1997). The resulting reconstruction was subjected to five cycles of refinement. Each cycle started with the appropriately CTF-modified reconstruction of the previous step, and the step size was 2°. The resolution of the reconstruction was calculated to be approximately 20 Å (Figure 5).

Preparation of Crystals

Crystals of *H. marismortui* 50S subunit were grown in high-salt buffers using PEG 6000 as a precipitant, as described by Yonath and coworkers (van Bohlen et al., 1991). They were grown in hanging drops by vapor diffusion at room temperature. The thin plates that resulted had maximum dimensions of 0.5 × 0.5 × 0.1 mm and were harvested after ∼2 weeks. Crystals were stabilized by gradual transfer into a solution containing ethylene glycol in addition to other components of the crystallization buffer and flash frozen in liquid propane. Heavy atom derivatives were prepared by soaking crystals in stabilization solutions containing the heavy atom compound of interest at a concentration of 1 mM for 1–6 days. In most cases, the diffraction properties of derivatized crystals did not change upon soaking in heavy atom solutions.

X-Ray Data Collection and Processing

All data were collected at the National Synchrotron Light Source (Brookhaven) from crystals frozen at 100 K, using beamlines X12c and X12b. For each heavy atom derivative, anomalous diffraction data were collected at the wavelength where peak anomalous scattering is observed. Diffraction data were recorded using either a 300 mm MAR imaging plate, or a Brandeis 2 × 2 CCD detector (W. C. Phillips, M. Stanton, D. O'Mara, C. Ingersoll, H. Qian, A. Stewart, and R. M. S., unpublished data) or a Quantum 4 CCD detector (Area Detector Systems Corporation). The beam size was 200 × 200 μm. The crystals were aligned along the long axis of the unit cell (570 Å) so that 1.5° oscillations could be used to collect reflections out to 7.0 Å resolution at the edge of the detector. The crystal-to-detector distances varied between 450.0 mm and 900.0 mm depending on crystal quality and beam divergence, and they were chosen so that maximum resolution data could be collected while avoiding overlapping of spots. Data sets were processed by using DENZO and SCALEPACK (Otwinowski, 1993).

Computational Techniques

The initial molecular replacement solution was obtained using an envelope derived from an EM reconstruction of the *E. coli* 50S subunit (see above). The map was stored as an array of densities, $\rho(x,y,z)$, on an arbitrary scale, sampled along all three directions at equal intervals, which were ∼1/3 of the calculated maximum resolution of the map. The map was reduced to a three-dimensional step function by assigning unit weight to all points of the array for which $\rho(x,y,z)$ was greater than some minimum value and setting all other points to zero. For the purposes of further computation, it was represented as a collection of atoms within the envelope. Direct rotational searches, based on the Patterson correlation coefficient (Huber, 1985; Brünger, 1990, 1997), were performed using X-PLOR (Brünger, 1992) and CNS (Brünger et al., 1998). In these searches, the linear scale factor of the reconstruction (the sampling interval) was varied, as was the threshold at which the envelope was defined. These two parameters are not completely independent because calculated structure factors depend primarily on the outer envelope, as noted previously (Jack et al., 1975). The orientations determined this way were subjected to Patterson correlation coefficient refinement using data between 100 and 30 Å. The results that yielded

(c) A stereo close-up of a 9 Å resolution density map showing the region that includes ribosomal protein L1; a backbone ribbon model of part of the 5S RNA is shown adjacent for scale. The upper part of the density contains ribosomal protein L1, and the rest may represent rRNA that interacts with L1. The yellow cage is at a lower contour level than the solid blue. The figure was generated with RIBBONS (Carson, 1991).

relatively high-correlation coefficients were used for translation function searches (Fujinaga and Read, 1987).

MIRAS Phasing

The heavy atom positions for the major binding sites were determined from combination difference anomalous and isomorphous Patterson maps at various resolution ranges. Solutions were cross-checked using anomalous and isomorphous difference Fourier maps, based on EM-derived phases. Refinement of the heavy atom cluster compound parameters was performed by maximum likelihood minimization of the lack of closure. All atoms in each of the clusters were included. Anomalous scattering was assumed to result only from heavy atoms in the cluster. All aspects of the isomorphous phasing including difference Patterson, difference Fourier map calculation, and heavy atom cluster rigid body refinement against lack of closure were done using the CNS program package (Brünger et al., 1998). Temperature factors were maintained at 40 $Å^2$ for all atoms in each of the clusters, while occupancies were refined as a group, and positions of atoms in clusters were refined as rigid bodies.

Acknowledgments

We thank Lu Min, Szilvia Szép, and Malcolm Capel (Brookhaven) for help with the X-ray data collection; Michael Pope and Gerta Sazani (George Washington University), Nevenka Brničević (Ruđer Bošković Institute, Croatia), and Duward F. Shriver and Nicolas Prokopuk (Northwestern University) for gifts of heavy atom cluster compounds; Axel Brünger for advice on molecular replacement procedures and heavy atom cluster refinement; Jimin Wang for helpful suggestions; and Doryen Bubeck and Rajendra Agrawal for assistance with image processing of electron micrographs and discussions. This work was supported by NIH grants GM-22778 to T. A. S., GM-54216 to P. B. M., and GM-29169 to J. F. N. B. was supported by a postdoctoral fellowship from the Cancer Research Fund of the Damon Runyon–Walter Winchell Foundation and P. N. by a grant from the Danish Research Council. Computing support for J. F. was provided by the National Center for Supercomputer Applications, University of Illinois at Urbana-Champaign.

Received April 1, 1998; revised May 6, 1998.

References

Agrawal, R.K., Penczek, P., Grassucci, R.A., Li, Y., Leith, A., Nierhaus, K.H., and Frank, J. (1996). Direct visualization of A-, P-, and E-site transfer RNAs in the *Escherichia coli* ribosome. Science *271*, 1000–1002.

Beckmann, R., Bubeck, D., Grassucci, R., Penczek, P., Verschoor, A., Blobel, G., and Frank, J. (1997). Alignment of conduits for the nascent polypeptide chain in the ribosome–Sec61 complex. Science *278*, 2123–2126.

Böttcher, B., Wynne, S.A., and Crowther, R.A. (1997). Determination of the fold of the core protein of hepatitis B virus by electron cryomicroscopy. Nature *386*, 88–91.

Brünger, A.T. (1990). Extension of molecular replacement: a new search strategy based on Patterson correlation refinement. Acta Crystallogr. *A46*, 46–57.

Brünger, A. (1992). X-PLOR Version 3.1. System for X-Ray Crystallography and NMR (New Haven, CT: Yale University Press).

Brünger, A.T. (1997). Patterson correlation searches and refinement. Methods Enzymol. *276*, 558–580.

Brünger, A.T., Adams, P.D., Clore, G.M., DeLano, W.L., Gros, P., Grosse-Kunstleve, R.W., Jiang, J.-S., Kuszewski, J., Nilges, M., Pannu, N.S., et al. (1998). Crystallography and NMR system (CNS): a new software suite for macromolecular structure determination. Acta Crystallogr., in press.

Capel, M.S., Engelman, D.M., Freeborn, B.R., Kjeldgaard, M., Langer, J.A., Ramakrishnan, V., Schindler, D.G., Schneider, D.K., Schoenborn, B.P., Sillers, I.-Y., et al. (1987). A complete mapping of the proteins in the small ribosomal subunit of *E. coli*. Science *238*, 1403–1406.

Carson, M. (1991). Ribbons 2.0. J. Appl. Crystallogr. *13*, 458–961.

Correll, C.C., Freeborn, B., Moore, P.B., and Steitz, T.A. Metals, motifs, and recognition in the crystal structure of a 5S rRNA domain. (1997). Cell *91*, 705–712.

Dube, P., Wieske, M., Stark, H., Schatz, M., Stahl, J., Zemlin, F., Lutsch, G., and van Heel, M. (1998). The 80S rat liver ribosome at 25 Å resolution by electron cryomicroscopy and angular reconstitution. Structure *6*, 389–399.

Dubochet, J., Adrian, M., Chang, J.-J., Homo, J.-C., Lepault, J., McDowall, A.W., and Schultz, P. (1988). Cryo-electron microscopy of vitrified specimens. Q. Rev. Biophys. *21*, 129–228.

Eisenstein, M., Hardesty, B., Odom, O.W., Kudlicki, W., Kramer, G., Arad, T., Franceschi, F., and Yonath, A. (1994). Modeling and experimental study of the progression of nascent proteins in ribosomes. In Biophysical Methods in Molecular Biology, G. Pifat, ed. (Rehovot, Israel: Balaban Press), pp. 213–246.

Franceschi, F., Weistein, S., Evers, U., Arndt, E., Jahn, W., Hansen, H.A.S., von Bohlen, K., Berkovitch-Yellin, Z., Eisenstein, M., Agmon, I., et al. (1993). Towards atomic resolution of prokaryotic ribosomes: crystallographic, genetic and biochemical studies. In The Translational Apparatus, K.H. Nierhaus, F. Franceschi, A.R. Subramanian, V.A. Erdmann, and B. Wittmann-Liebold, eds. (New York: Plenum Press), pp. 397–410.

Frank, J., Zhu, J., Penczek, P., Li, Y., Srivastava, S., Verschoor, A., Radermacher, M., Grassucci, R., Lata, R.K., and Agrawal, R.K. (1995a). A model for protein synthesis based on cryo-electron microscopy of the *E. coli* ribosome. Nature *376*, 441–444.

Frank, J., Verschoor, A., Li, Y., Zhu, J., Lata, R.K., Radermacher, J., Penczek, P., Grassucci, R., Agrawal, R.K., and Srivastava, S. (1995b). A model of the translational apparatus based on a three-dimensional reconstruction of the *Escherichia coli* ribosome. Biochem. Cell Biol. *73*, 757–765.

Fujinaga, M., and Read, R.J. (1987). Experiences with a new translation-function program. J. Appl. Crystallogr. *20*, 517–521.

Huber, R. (1985). In Molecular Replacement, Proceedings of the Daresbury Study Weekend, Daresbury, February, P.A. Mochin, ed. (Daresbury, United Kingdom: Science and Engineering Research Council, The Librarian, Daresbury Laboratory), pp. 58–61.

Jack, A., Harrison, S.C., and Crowther, R.A. (1975). Structure of tomato bushy stunt virus II. Comparison of results obtained by electron microscopy and X-ray diffraction. J. Mol. Biol. *97*, 163–172.

Knablein, J., Neuefeind, T., Schneider, F., Bergner, A., Messerschmidt, A., Lowe, J., Steipe, B., and Huber, R. (1997). $Ta_6Br^{(2+)}_{12}$, a tool for phase determination of large biological assemblies by X-ray crystallography. J. Mol. Biol. *270*, 1–7.

Ladenstein, R., Bacher, A., and Huber, R. (1987). Some observations of a correlation between the symmetry of large heavy-atom complexes and their binding sites on proteins. J. Mol. Biol. *195*, 751–753.

Lata, K.R., Agrawal, R.K., Penczek, P., Grassucci, R., Zhu, J., and Frank, J. (1996). Three-dimensional reconstruction of the *Escherichia coli* 30S ribosomal subunit in ice. J. Mol. Biol. *262*, 43–52.

Leonard, K.R., and Lake, J.A. (1979). Ribosome structure: hand determination by electron microscopy of 30S subunit. J. Mol. Biol. *128*, 155–163.

Malhotra, A., and Harvey, S.C. (1994). A quantitative model of the *Escherichia coli* 16S RNA in the 30S ribosomal subunit. J. Mol. Biol. *240*, 308–340.

Malhotra, A., Penczek, P., Agrawal, R.K., Gabashvili, I.S., Grassucci, R.A., Jünemann, R., Burkhardt, N., Nierhaus, K.H., and Frank, J. (1998). *Escherichia coli* 70S ribosome at 15 Å resolution by cryo-electron microscopy: localization of fMet-$tRNA_f^{Met}$ and fitting of L1 protein. J. Mol. Biol., in press.

May, R.P., Nowotny, V., Nowotny, P., Voss, H., and Nierhaus, K.H. (1992). Inter-protein distances within the large subunit from *Escherichia coli* ribosomes. EMBO J. *11*, 373–378.

Milligan, R.A., and Unwin, P.N.T. (1986). Location of exit channel for nascent protein in 80S ribosome. Nature *319*, 693–695.

Mueller, F., and Brimacombe, R. (1997a). A new model for the three-dimensional folding of *Escherichia coli* 16S ribosomal RNA. I. Fitting the RNA to a 3D electron microscopic map at 20 Å. J. Mol. Biol. *271*, 524–544.

Mueller, F., and Brimacombe, R. (1997b). A new model for the three-dimensional folding of *Escherichia coli* 16S ribosomal RNA. II. The RNA–protein interaction data. J. Mol. Biol. *271*, 545–565.

Mueller, F., Stark, H., van Heel, M., Rinke-Appel, J., and Brimacombe, R. (1997). A new model for the three-dimensional folding of *Escherichia coli* 16S ribosomal RNA. III. The topography of the functional center. J. Mol. Biol. *271*, 566–587.

Neuefeind, T., Bergner, A., Schneider, F., Messerschmidt, A., and Knablein, J. (1997). The suitability of Ta6Br12(2+) for phasing in protein crystallography. Biol. Chem. *378*, 219–221.

Noller, H.F., Hoffarth, V., and Zimniak, L. (1992). Unusual resistance of peptidyl transferase to protein extraction procedures. Science *256*, 1416–1419.

Noller, H.F., Green, R., Heilek, G., Hoffarth, V., Huttenhofer, A., Joseph, S., Lee, I., Lieberman, K., Mankin, A., Merryman, C., et al. (1995). Structure and function of ribosomal RNA. Biochem. Cell Biol. *73*, 997–1009.

Oakes, M., Henderson, E., Scheinman, A., Clark, M., and Lake, J.A. (1986). Ribosome structure, function, and evolution: mapping ribosomal RNA, proteins, and functional sites in three dimensions. In Structure, Function and Genetics of Ribosomes, B. Hardesty and G. Kramer, eds. (New York: Springer-Verlag), pp. 47–67.

O'Halloran, T.V., Lippard, S.J., Richmond, T.J., and Klug, A. (1987). Multiple heavy-atom reagents for macromolecular X-ray structure determination. Application to the nucleosome core particle. J. Mol. Biol. *194*, 705–712.

Otwinowski, Z. (1993). DENZO. In Data Collection and Processing, L. Sawyer, N. Isaacs, and D. Bailey, eds. (Warrington, England: SERC Daresbury Laboratory), pp 56–62.

Penczek, P., Grassucci, R.A., and Frank. J. (1994). The ribosome at improved resolution: new techniques for merging and orientation refinement in 3D cryo-electron microscopy of biological particles. Ultramicroscopy *53*, 251–270.

Podjarni, A.D., and Urzhumtsev, A.G. (1997). Low resolution Phasing. Methods Enzymol. *276*, 641–658.

Radermacher, M., Wagenknecht, T., Verschoor, A., and Frank, J. (1987). Three-dimensional reconstruction from a single-exposure, random conical tilt series applied to the 50S ribosomal subunit. J. Microsc. *146*, 113–136.

Rossmann, M.G. (1995). Ab initio phase determination and phase extension using non-crystallographic symmetry. Curr. Opin. Struct. Biol. *5*, 650–655.

Schlunzen, F., Hansen, H.A.S., Thygesen, J., Bennett, W.S., Volkmann, N., Levin, I., Harms, J., Bartles, H., Zaytzev-Bashan, A., Berkovitch-Yellin, Z., et al. (1995). A milestone in ribosomal crystallography: the construction of preliminary electron density maps at intermediate resolution. Biochem. Cell Biol. *73*, 739–749.

Shevack, A., Gewitz, H.S., Hennemann, B., Yonath, A., and Wittmann, H.G. (1985). Characterization and crystallization of ribosomal particles from *Haloarcula marismortui*. FEBS Lett. *184*, 68–71.

Stark, H., Mueller, F., Orlova, E.V., Schatz, M., Dube, P., Erdemir, T., Zemlin, F., Brimacombe, R., and van Heel, M. (1995). The 70S *Escherichia coli* ribosome at 23 Å resolution: fitting the ribosomal RNA. Structure *3*, 815–821.

Stark, H., Orlova, E.V., Rinke-Appel, J., Junke, N., Mueller, F., Rodnina, M., Wintermeyer, W., Brimacombe, R., and van Heel, M. (1997a). Arrangment of tRNAs in pre- and posttranslocational ribosomes revealed by electron cryomicroscopy. Cell *88*, 19–28.

Stark, H., Rodnin, M.V., Rinke-Appel, J., Brimacombe, R., Wintermeyer, W., and van Heel, M. (1997b). Visualization of elongation factor Tu on the *Escherichia coli* ribosome. Nature *389*, 403–406.

Stoeffler, G., and Stoeffler-Meilicke, M. (1986). Immuno electron microscopy on *Escherichia coli* ribosomes. In Structure, Function, and Genetics of Ribosomes, B. Hardesty and G. Kramer, eds. (New York: Springer-Verlag), pp. 28–46.

Thygesen, J., Weinstein, S., Franceschi, F., and Yonath, A. (1996). The suitability of multi-metal clusters for phasing in crystallography of large macromolecular assemblies. Structure *4*, 513–518.

van Bohlen, K., Makowski, I., Hansen, H.A.S., Bartels, H., Berkovitch-Yellin, Z., Zaytzev-Bushan, A., Meyer, S., Paulke, C., Franscheschi, F., and Yonath, A. (1991). Characterization and preliminary attempts for derivatization of crystals of large ribosomal subunits from *Haloarcula marismortui* diffracting to 3 Å resolution. J. Mol. Biol. *222*, 11–15.

Verschoor, A., Warner, J.R., Srivastava, S., Grassucci, R.A., and Frank, J. (1998). Three-dimensional structure of the yeast ribosome. Nucleic Acids Res. *26*, 655–661.

Wagenknecht, T., Grassucci, R., and Frank. J. (1988). Electron microscopy and computer image averaging of ice-embedded large ribosomal subunits from *E. coli*. J. Mol. Biol. *199*, 137–147.

Wittmann-Liebold, B. (1986). Ribosomal proteins: their structure and evolution. In Structure, Function, and Genetics of Ribosomes, B. Hardesty and G. Kramer, eds. (New York: Springer-Verlag), pp. 326–361.

Wittmann-Liebold, B., Kopke, A.K.E., Arndt, E., Kromer, W., Hatakeyama, T., and Wittmann, H.G. (1990). Sequence comparison and evolution of ribosomal proteins and their genes. In The Ribosome: Structure, Function, and Genetics, W.E. Hill, A. Dahlberg, R.A. Garrett, P.B. Moore, D. Schlessigner, and J.R. Warner, eds. (Washington, D.C.: American Society for Microbiology), pp. 598–616.

Woese, C.R. (1996). The world of ribosomal RNA. In Ribosomal RNA: Structure, Evolution, Processing, and Function in Protein Biosynthesis, R.A. Zimmermann and A. E. Dahlberg, eds. (Boca Raton: CRC Press, Inc.), pp. 23–48.

Yonath, A., Mussig, J., Tesche, B., Lorenz, S., Erdmann, V.A., and Wittmann, H.G. (1980). Crystallization of the large ribosomal subunits from *Bacillus stearothermophilus*. Biochem. Int. *1*, 428–435.

Yonath, A., Leonard, K.R., and Wittmann, H.G. (1987). A tunnel in the large ribosomal subunit revealed by three-dimensional reconstruction. Science *23*, 813–816.

Zhu, J., Penczek, P.A., Schroeder, R., and Frank, J. (1997). Three-dimensional reconstruction with contrast transfer function correction from energy-filtered cryoelectron micrographs: procedure and application to the 70S *Escherichia coli* ribosome. J. Struct. Biol. *118*, 197–219.